Original scientific papers UDK 616.1−089.84:616−127
doi: 10.7251/COMEN1602099F

EXPERIMENTAL TESTING AND NUMERICAL MODELLING OF STENTS IN THE CORONARY ARTERIES

Nenad Filipović[1,2,], Dalibor Nikolić[1,2], Igor Saveljić[1,2], Themis Exarchos[3], Oberdan Parodi[4]*

[1] Faculty of Engineering, University of Kragujevac, Sestre Janjića 6, Kragujevac, Serbia
[2] BioIRC, Bioengineering Research and Development Center, Prvoslava Stojanovića 6, Kragujevac, Serbia
[3] Foundation of Research and Technology Hellas-Biomedical Research Institute, University of Ioannina, Ioannina, Greece
[4] Instituto di Fisiologia Clinica, Consiglio Nazionale delle Ricerche (IFC CNR), Pisa, Italy

Abstract: In this study, experimental and numerical stent modelling with plaque formation and progression for specific patient in the coronary arteries is described. In the method, section experimental stent testing is firstly described. Then numerical methods with finite element methods are given. Blood flow simulation is described with Navier-Stokes and continuity equation. Blood vessel wall is modelled with nonlinear viscoelastic material properties. The coupling of fluid dynamics and solute dynamics at the endothelium was achieved by the Kedem-Katchalsky equations. The inflammatory process is modelled using three additional reaction-diffusion partial differential equations. In the results section, the examples with rigid and deformable arterial wall with stented and unstented arteries are presented. Effective stress analysis results for stent deployment have been shown. These experimental and numerical methods can give better understanding of stent deployment procedure and arterial wall response in everyday clinical practice.

Keywords: stent testing, experimental, numerical, stent deployment simulation, finite element method.

1. INTRODUCTION

Each year, millions of individuals are affected by CAD worldwide. Given the high burden of the disease, it is important to develop innovative technologies that can improve outcomes and disease management. Stenting for coronary applications has been widely adopted in clinical practice worldwide, and can be used in a wide range of indications. Among the different types of stents available, drug-eluting stenting dominates the market. By 2020, the coronary stents market for drug-eluting and bioabsorbable stenting is estimated to be over $5.61 billion.

Restenosis is the excessive growth of new tissue in the stented segment which can reblock the artery. The success of the stenting procedure depends on the severity of the restenosis. Neointimal hyperplasia has been shown to be dependant on several factors including arterial injury, areas of flow induced low WSS less than 0.5 N/m2, areas of flow-induced high wall shear stress gradients (WSSG) higher than 200 N/m3, as well as other patient-specific medical factors such as diabetes mellitus [1−5,6]. The evaluation of haemodynamic changes caused by a stent implantation is thus important to minimize those negative biological effects and to optimise the stent design. Beside experimental investigations using particle image velocimetry [7], computational fluid dynamics (CFD) has been used extensively to predict increased areas of low WSS and high WSSG in stented arteries [5,7,9−18].

CFD techniques have the advantage of a greater flexibility and easiness of use with respect to the experimental or in vivo methods. They can provide detailed information on critical local flow parameters near the stent struts and the arterial wall which

* Corresponding author: fica@kg.ac.rs

are not accessible in biological flows. However, modelling often has its own limitations in the form of simplifications to the real problem. Many computational studies in the literature dealt with the influence of stent physical parameters on fluid dynamical changes correlated with the restenosis process [5,7,10−12,14−16,18]. Stent strut spacing, thickness and number of struts were found to influence the distribution of low and high shear stress values. However, the unrealistic assumption in the computational models that the stented artery is a simple cylindrical, rigid tube or even flat plane is implicit to most of these investigations. In reality, the coronary vasculature within which stents are commonly deployed, exhibits a highly complex geometry with extensive curvature. This vessel curvature can have significant effect on the skewness of the velocity profile and the general behaviour of the flow in the stented segment.

A first attempt to consider the effect of vascular concentricity was done by comparing two 3D models of vessel and stent [17]. The artery had a circular cross-section in the first model whereas it was conformed to the stent geometry in the other model, thus resulting in a polygonal or straightened shape. Circumferential straightening introduced areas of high WSS among stent struts that were absent in the stented vessel model with circular cross-section, but the geometry of an atherosclerotic lesion after stent implantation may vary based on lesion composition. The purpose of another computational study was to investigate the extent of fluid mechanical disturbance induced by the presence of a stent within straight and curved arterial segments [13]. The presented results suggest that in the presence of a stent, the relative magnitudes of the wall shear stress along the inner and outer walls of a curved arterial segment depend in a complex fashion on the vessel curvature as well as the Reynolds number and may be difficult to be predicted a priori.

All simulations reported have assumed that both the arterial wall and the stent are rigid. This assumption was justified with a hardening of the arterial wall due to the formation of calcified plaque in advanced artheriosclerosis and the stenting of the vessel, so that the compliance of the wall at the site of stent deployment is expected to be relatively low. Further limitation of many investigations is a simplified, purely geometrical modelling of the stent struts or wires lacking a description of the realistic stent geometry after its deployment. Such a realistic geometrical representation of the deployed stent is particularly important in the case of a stenosed artery where the shape of the plaque that is pushed outwards by the stent is far from being geometrically simple or ideal in shape. Another geometric limitation of those studies is the fact that the composition of the atherosclerotic plaque has not been taken into consideration so far. The composition of the plaque can significantly affect the inner geometry of the lumen and result in an asymmetric stent expansion. Some studies have, therefore, performed a physical stent deployment as a basis for the fluid dynamic analysis to obtain a more realistic stent pattern [7,9,18]. In none of the reported investigations, the geometry of the stented artery is a realistic reproduction of a patient-specific stenosed artery which underwent a stenting procedure.

This paper is organized as follows. We firstly described experimental stent testing according to ISO 25539-1. Then some numerical methods for simulation of blood flow, deformable arterial wall as well as plaque formation and development are described. Some results for coronary blood vessel and stent deployment are presented. Finally, discussion and conclusions are given.

2. METHODS

2.1. Experimental stent testing

The design of a new stent requires mechanical stent testing performed according to ISO 25539-1, Cardiovascular implants - Endovascular devices. As an example, there is a test for the evaluation of the durability of the stent product. The test can evaluate the durability of the stent with respect to the product specifications by recreating the type of loading conditions seen clinically during a 400-million-cycle simulation conducted at the targeted testing speed of 35Hz. Once implanted, the stent will initially experience an initial load due to the reduction of device diameter when it is placed inside the vessel. The stent will also experience a cyclical loading due to the dynamics of pulsatile flow and the resulting compliant nature of the vessel. This will cause the diameter of the stent to expand and contract with the vessel wall. In order to recreate the type and magnitude of loading conditions seen clinically, the Dynatek SVP24 accelerated durability test (Figure 1) is used. SVP24 forces fluid into and out of compliant conduits (mock vessels), which forces mock vessels containing test-samples to expand and collapse radially, thus simulating the type of motion and loads that stent would face *in vivo*. The SVP test fixture is ported in a way that pressures can be measured at both ends of the device simultaneously. The SVP test fixture automatically controls temperature as well as systemic pressure. The pressure differen-

ce is controlled by the signal amplitude to the hyperdrive motor driving the bellows. Speed, cycle counts, and intermittent pressure traces are all automatically controlled by a computer. This is consistent with standard for test methods for Endovascular Prostheses (ISO 25539-1 and ISO 25539-2) and ASTM F2477.

Figure 1. Dynatek SVP24 accelerated durability tester (ISO 25539-1)

Certain aspects of the test may be considered more aggressive than the normal physiological conditions the stent would face in clinical practice. This test protocol was developed to comply with ISO 25539-1, ISO 25539-2, and ASTM F2477, which are the standards developed for fatigue testing of conventional stents. Conventional stents operate under qualitatively different and more aggressive loading conditions than the embolization devices as they are exposed to the full extent of the systemic pulsatile blood pressure throughout their service life. The following addresses the key parameters that impact the loading conditions and their relevance to the normal clinical conditions: Preload (oversizing, preload) Test-samples are placed into mock vessels, which is considered to be the worst-case IFU vessel size with respect to embolic frame durability per REP-EPE-0010-00R01 – Finite Element Analysis 2.0& Preliminary Fatigue Prediction. Radial Compliance (cyclic load) The mock vessels are specifically designed to have a radial compliance in the range of 5-7% per 100mmHg. This cyclic load level is consistent with standards ISO 25539-2 and ASTM F2477. Systolic/Diastolic Pressures The testing is carried out at normal physiological systolic and diastolic pressures (120±5/80±5mmHg) on proximal end of the device. Testing Speed This test is conducted at the accelerated targeted testing speed of 35Hz. While the targeted testing speed is 35Hz, the actual testing speed may have to be adjusted slightly in order to meet the pressure specification of 120±5/80±5mmHg. The accelerated testing speed may introduce some phenomena that are not clinically relevant and which can influence the fatigue performance evaluation. Accelerated testing often induces excessive device/device component movement and other resonance-related and not physiologically relevant phenomena. All of those conditions are not expected clinically and may induce non-physiologically relevant failure modes. Contact between test samples and internal wall of the mock vessels The accelerated testing speed produces the exaggerated relative movement of the device with reference to the mock vessel, which produces an aggressive interaction between the device and mock vessel wall. Due to the relatively abrasive nature of the internal wall of the mock vessels, if conducted at the accelerated testing speed, this testing represents overload conditions with respect to coating wear, especially along the line of contact. Environment The testing occurs with pH 7.4 phosphate buffered saline with added antimicrobial on the inside of test samples. Testing is carried out at 37° C. Fatique Simulation This testing represents approximately 10-year-service life simulation consisting of 400 million cycles.

2.2. Blood flow simulation

In general, the sequence used to perform blood flow simulations is the acquisition of the 3D reconstructed model from the image modalities, the application of the appropriate input data, and finally, the acquisition of the desired output. Blood flow simulations are performed in three different categories of arteries: a) In unstented arteries assuming the walls to be rigid, b) in unstented arteries with deformable walls and c) in stented arteries with rigid walls.

The blood can be considered as an incompressible homogenous viscous fluid for flow in large blood vessels. Also, the laminar flow is dominant in physiological flow environment. Therefore, the fundamental laws of physics which include balance of mass and balance of linear momentum are applicable here. These laws are expressed by continuity equation and the Navier-Stokes equations.

We here present the final form of these equations to emphasize some specifics related to blood flow. The incremental-iterative balance equation of a finite element for a time step 'n' and equilibrium iteration 'i' has a form

$$\begin{bmatrix} \frac{1}{\Delta t}\mathbf{M} + {}^{n+1}\tilde{\mathbf{K}}_{vv}^{(i-1)} & \mathbf{K}_{vp} \\ \mathbf{K}_{vp}^{T} & \mathbf{0} \end{bmatrix} \begin{Bmatrix} \Delta\mathbf{V}^{(i)} \\ \Delta\mathbf{P}^{(i)} \end{Bmatrix}_{blood} = \begin{Bmatrix} {}^{n+1}\mathbf{F}_{ext}^{(i-1)} \\ 0 \end{Bmatrix} - \begin{bmatrix} \frac{1}{\Delta t}\mathbf{M} + {}^{n+1}\mathbf{K}^{(i-1)} & \mathbf{K}_{vp} \\ \mathbf{K}_{vp}^{T} & 0 \end{bmatrix} \begin{Bmatrix} {}^{n+1}\mathbf{V}^{(i-1)} \\ {}^{n+1}\mathbf{P}^{(i-1)} \end{Bmatrix} + \begin{Bmatrix} \frac{1}{\Delta t}\mathbf{M}\,{}^{n}\mathbf{V} \\ 0 \end{Bmatrix} \tag{1}$$

where ${}^{n+1}\mathbf{V}^{(i-1)}$ ${}^{n+1}\mathbf{P}^{(i-1)}$ are the nodal vectors of blood velocity and pressure, with the increments in time step $\Delta\mathbf{V}^{(i)}$ and $\Delta\mathbf{P}^{(i)}$ (the index 'blood' is used to emphasize that we are considering blood as the fluid); Δt is the time step size and the left upper indices 'n' and 'n+1' denote start and end of time step; and the matrices and vectors are defined in [19]. Note that the vector ${}^{n+1}\mathbf{F}_{ext}^{(i-1)}$ of external forces includes the volumetric and surface forces. In the assembling of these equations, the system of equations of the form (1) is obtained, with the volumetric external forces and the surface forces acting only on the fluid domain boundary (the surface forces among the internal element boundaries cancel).

The specifics for the blood flow are that the matrix ${}^{n+1}\mathbf{K}^{(i-1)}$ may include variability of the viscosity if non-Newtonian behavior of blood is considered. We have that

$$\left[K_{KJ}^{(i-1)}\right]_{mk} = \left[\hat{K}_{KJ}^{(i-1)}\right]_{mk} + \int_{V} \mu^{(i-1)} N_{K,j} N_{J,j}\, dV \tag{2}$$

where $\mu^{(i-1)}$ corresponds to the constitutive law for the last known conditions (at iteration '$i-1$'). In case of use of the Cason relation (2), the second invariant of the strain rate $D_{II}^{(i-1)}$ is to be evaluated when computing $\mu^{(i-1)}$.

We note here that the penalty method can also be used, as well as the ALE formulation in case of large displacements of blood vessel walls [20].

In addition to the velocity and pressure fields of the blood, the distribution of stresses within the blood can be evaluated. The stresses ${}^{t}\sigma_{ij}$ at time 't' follow from

$${}^{t}\sigma_{ij} = -{}^{t}p\,\delta_{ij} + {}^{t}\sigma_{ij}^{\mu} \tag{3}$$

where

$${}^{t}\sigma_{ij}^{\mu} = {}^{t}\mu\left(v_{i,j} + v_{j,i}\right) \tag{4}$$

is the viscous stress. Here, ${}^{t}\mu$ is viscosity corresponding to the velocity vector ${}^{t}\mathbf{v}$ at a spatial point within the blood domain. The field of the viscous stresses is given by (4).

Further, the wall shear stress at the blood vessel wall is calculated as:

$${}^{t}\tau = {}^{t}\mu\frac{\partial\, {}^{t}v_{t}}{\partial n} \tag{5}$$

where ${}^{t}v_{t}$ denotes the tangential velocity, and n is the normal direction at the vessel wall. Practically, we first calculate the tangential velocity at the integration points near the wall surface, and then numerically evaluate the velocity gradient $\partial\, {}^{t}v_{t} / \partial n$; finally, we determine the viscosity coefficient ${}^{t}\mu$ using the average velocity at these integration points. In essence, the wall shear stress is proportional to the shear rate γ at the wall, and the blood dynamic viscosity μ.

For a pulsatile flow,the mean wall shear stress within a time interval T can be calculated as [21]

$${}^{T}\tau_{mean} = \left|\frac{1}{T}\int_{0}^{T} {}^{t}\tau_{n}\, dt\right| \tag{6}$$

Another scalar quantity is a time-averaged magnitude of the surface traction vector, calculated as

$${}^{T}\tau_{mag} = \frac{1}{T}\int_{0}^{T} \left|{}^{t}\mathbf{t}\right| dt \tag{7}$$

where the vector ${}^{t}\mathbf{t}$ is given by the Cauchy formula.

2.3. Modeling the deformation of blood vessels

Blood vessel tissue has complex mechanical characteristics. The tissue can be modeled by using various material models, from linear elastic to nonlinear viscoelastic. We here summarize the governing finite element equations used in modeling wall tissue deformation with emphasis on implementation of nonlinear constitutive models.

The finite element equation of balance of linear momentum is derived from the fundamental differential equations of balance of forces acting at an elementary material volume. In dynamic analysis we include the inertial forces in this equation. Then, by applying the principle of virtual work

$$\mathbf{M}\ddot{\mathbf{U}} + \mathbf{B}^{w}\dot{\mathbf{U}} + \mathbf{K}\mathbf{U} = \mathbf{F}^{ext} \tag{8}$$

Here the element matrices are: $\mathbf{M}$ is mass matrix; $\mathbf{B}^{w}$ is the damping matrix, in case when the material has a viscous resistance; $\mathbf{K}$ is the stiffness matrix; and $\mathbf{F}^{ext}$ is the external nodal force vector which includes body and surface forces acting on the element. By the standard assembling procedure, the dynamic differential equations of motion are obtained. These differential equations can further be inte-

grated in a way described, with a selected time step size Δt. The nodal displacements ${}^{n+1}\mathbf{U}$ at end of time step are finally obtained according to equation:

$$\hat{\mathbf{K}}_{tissue}\,{}^{n+1}\mathbf{U} = {}^{n+1}\hat{\mathbf{F}} \tag{9}$$

where the tissue stiffness matrix $\hat{\mathbf{K}}_{tissue}$ and vector ${}^{n+1}\hat{\mathbf{F}}$ are expressed in terms of the matrices and vector in (8). Note that this equation is obtained under the assumption that the problem is linear: displacements are small, the viscous resistance is constant, and the material is linear elastic.

In many circumstances of blood flow, the wall displacements can be large, as in case of aneurism or hart, hence the problem becomes geometrically nonlinear. Also, the tissues of blood vessels have nonlinear constitutive laws, leading to materially-nonlinear FE formulation. Therefore, the approximations adopted to obtain equation (9) may not be appropriate. For a nonlinear problem, instead of (9) we have the incremental-iterative equation

$${}^{n+1}\hat{\mathbf{K}}_{tissue}^{(i-1)}\,\Delta\mathbf{U}^{(i)} = {}^{n+1}\hat{\mathbf{F}}^{(i-1)} - {}^{n+1}\mathbf{F}^{\mathrm{int}(i-1)} \tag{10}$$

where $\Delta\mathbf{U}^{(i)}$ are the nodal displacement increments for the iteration 'i', and the system matrix ${}^{n+1}\hat{\mathbf{K}}_{tissue}^{(i-1)}$, the force vector ${}^{n+1}\hat{\mathbf{F}}^{(i-1)}$ and the vector of internal forces ${}^{n+1}\mathbf{F}^{\mathrm{int}(i-1)}$ correspond to the previous iteration.

We here emphasize the material nonlinearity of blood vessels which is used in further applications. As presented, the geometrically linear part of the stiffness matrix, $\left({}^{n+1}\mathbf{K}_L\right)_{tissue}^{(i-1)}$, and nodal force vector, ${}^{n+1}\mathbf{F}^{\mathrm{int}(i-1)}$, are defined in equation:

$$\left({}^{n+1}\mathbf{K}_L\right)_{tissue}^{(i-1)} = \int_V \mathbf{B}_L^T\,{}^{n+1}\mathbf{C}_{tissue}^{(i-1)}\,\mathbf{B}_L\,dV, \quad \left({}^{n+1}\mathbf{F}^{\mathrm{int}}\right)^{(i-1)} = \int_V \mathbf{B}_L^T\,{}^{n+1}\boldsymbol{\sigma}^{(i-1)}\,dV \tag{11}$$

where the consistent tangent constitutive matrix ${}^{n+1}\mathbf{C}_{tissue}^{(i-1)}$ of tissue and the stresses at the end of time step ${}^{n+1}\boldsymbol{\sigma}^{(i-1)}$ depend on the material model used. Calculation of the matrix ${}^{n+1}\mathbf{C}_{tissue}^{(i-1)}$ and the stresses ${}^{n+1}\boldsymbol{\sigma}^{(i-1)}$ for the tissue material models used in further applications. In each of the subsequent sections we will give the basic data about the models used in the analysis.

2.4. Plaque formation and progression modelling – continuum approach

Continuum based methods is an efficient way for modelling the evolution of plaque. In our model, LDL concentration is first introduced into the system of partial differential equations as a boundary condition. The model simulates the inflammatory response formed at the initial stages of plaque formation.

Regarding the particle dynamics, the model is based on the involvement of LDL/oxidized LDL, monocytes and macrophages, and foam cells and extra cellular matrix. Reaction-diffusion differential equations are used to model these particle dynamics. The adhesion rate of the molecules depends on the local hemodynamics which is described by solving the Navier-Stokes equations. Intima LDL concentration is a function of the wall shear stress, while the adhesion of monocytes is a function of shear stress and VCAM. Finally, the alterations of the arterial wall are simulated. A finite element solver is used to solve the system of the equations. The lumen is defined as a 2D domain while the intima is simplified as 1D model due to its thin geometry. First, the LDL penetration to the arterial wall as well as the wall shear stress is calculated. Then the concentration of the various components of the model is calculated in order to simulate the intima fattening in the final step.

The LDL penetration is defined by the convection-diffusion equation, while the endothelial permeability is shear stress dependent. This model produces results about the initial stages of the atherosclerotic plaque formation. More specifically, concentration of LDL is calculated on the artery wall and in the next step the oxidized LDL. Furthermore, monocytes and their modified form (macrophages) are also counted. Solution to the system provides to the user the concentration of foam cells created when a threshold on LDL concentration is reached.

The previous model describes the initial stages of atherosclerosis. However, atherosclerosis is characterized by the proliferation of SMCs. A medical user needs a prediction for the plaque formation which is based on the concentration of SMCs, the necrotic core and the extracellular matrix. In this respect, a new approach to count the concentration of SMCs is being developed. The user is also provided with results regarding the formation of plaque in an overall manner.

The fluid is assumed to be steady, incompressible and laminar for modeling fluid dynamics in the lumen Navier-Stokes equations were used (12),(13)

$$-\mu\nabla^2 u_l + \rho\left(u_l\cdot\nabla\right)u_l + \nabla p_l = 0 \tag{12}$$

$$\nabla u_l = 0 \tag{13}$$

where u_l is blood velocity, p_l is pressure, μ is blood dynamic viscosity and ρ is blood density.

Darcy`s Law were used to model mass transfer across the wall (transmural flow) of the blood vessel.

$$u_w - \nabla\left(\frac{k}{\mu_p} p_w\right) = 0 \quad (14)$$

$$\nabla u_w = 0 \quad (15)$$

where u_w is transmural velocity, p_w pressure in the arterial wall, μ_p is viscosity of blood plasma, and k is the Darcian permeability coefficient of the arterial wall (14), (15). Convective diffusion equations were occupied for modeling mass transfer in the lumen (16)

$$\nabla\cdot\left(-D_l\nabla c_l + c_l u_l\right) = 0 \quad (16)$$

where c_l represents blood concentration in the lumen and D_l is diffusion coefficient of the lumen.

Convective diffusion reactive equations (17) were used for modeling mass transfer in the wall which are related to transmural flow.

$$\nabla\cdot\left(-D_w\nabla c_w + K c_w u_w\right) = r_w c_w \quad (17)$$

where c_w is solute concentration in the arterial wall, D_w is diffusive coefficient of solution in the wall, K is solute lag coefficient and r_w is consumption rate constant.

The coupling of fluid dynamics and solute dynamics at the endothelium was achieved by the Kedem-Katchalsky equations (18),(19).

$$J_v = L_p\left(\Delta p - \delta_d \Delta\pi\right) \quad (18)$$

$$J_s = P\Delta c + \left(1-\delta_f\right) J_v \bar{c} \quad (19)$$

where L_p is the hydraulic conductivity of the endothelium, Δc is the solute concentration difference across the endothelium, Δp is the pressure drop across the endothelium, $\Delta\pi$ is the oncotic pressure difference across the endothelium, σ_d is the osmotic reflection coefficient, σ_f is the solvent reflection coefficient, P is the solute endothelial permeability, and $\bar{c}$ is the mean endothelial concentration [22].

The inflammatory process is modeled using three additional reaction-diffusion partial differential equations [23]:

$$\begin{aligned} &\partial_t O = d_1\Delta O - k_1 O\cdot M \\ &\partial_t M + div(v_w M) = d_2\Delta M - k_1 O\cdot M + S/(1+S) \\ &\partial_t S = d_3\Delta S - \lambda S + k_1 O\cdot M + \gamma(O - O^{thr}) \end{aligned} \quad (20)$$

where O is the oxidized LDL in the wall, M and S are concentrations in the intima of macrophages and cytokines, respectively; d_1,d_2,d_3 are the corresponding diffusion coefficients; λ and γ are degradation and LDL oxidized detection coefficients; and v_w is the inflammatory velocity of plaque growth [23],[24].

3. RESULTS

Blood was taken as an incompressible Newtonian fluid, appropriate for larger arteries [19,23]. The blood density was ρ=1050 [kg/m^3], and the kinematic viscosity was ν=3.5e-6 [m^2/s].

All of above mention mechanical stent testing can be done very easy with computer simulation where different diameter, size, design, shape, material of stent can be testing much faster and cheaper than in-vitro mechanical testing.

Simulation of stent opening with cylinder with different radius is presented in Figure 2.

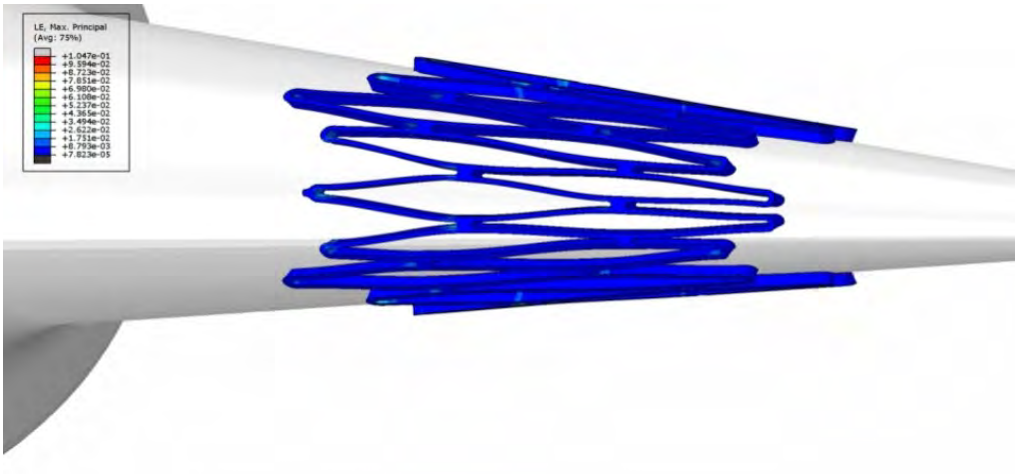

Figure 2. Simulation of stent opening with cylinder with different radius

The effective von Mises stress distribution in the stent which is opening with inflation pressure 1 MPa is presented in Figure 3. It can be observed that high stresses zones are located near the connectors between the stent struts. These parts are subjected to plastic deformation with maximal stress around 180 MPa.

We developed a method which enables a virtual stenting intervention in a patient-specific, stenosed artery. This highly complex physical problem includes all system components of stenting procedure, namely the stenosed artery, the stent und the balloon to inflate the stent. A virtual positioning in the reconstructed artery is performed before the balloon is gradually inflated, widens the stent in radial direction which enables a dilation of the stenosed artery (Figure 4).

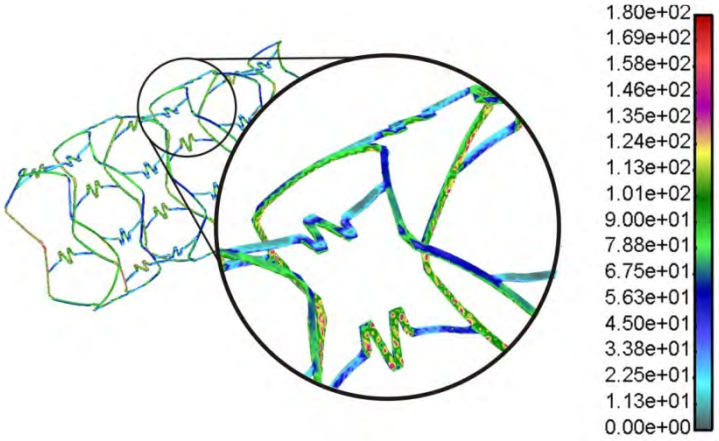

Figure 3. Effective von Mises stress distribution for inflation pressure of 1 MPa. The units are in MPa

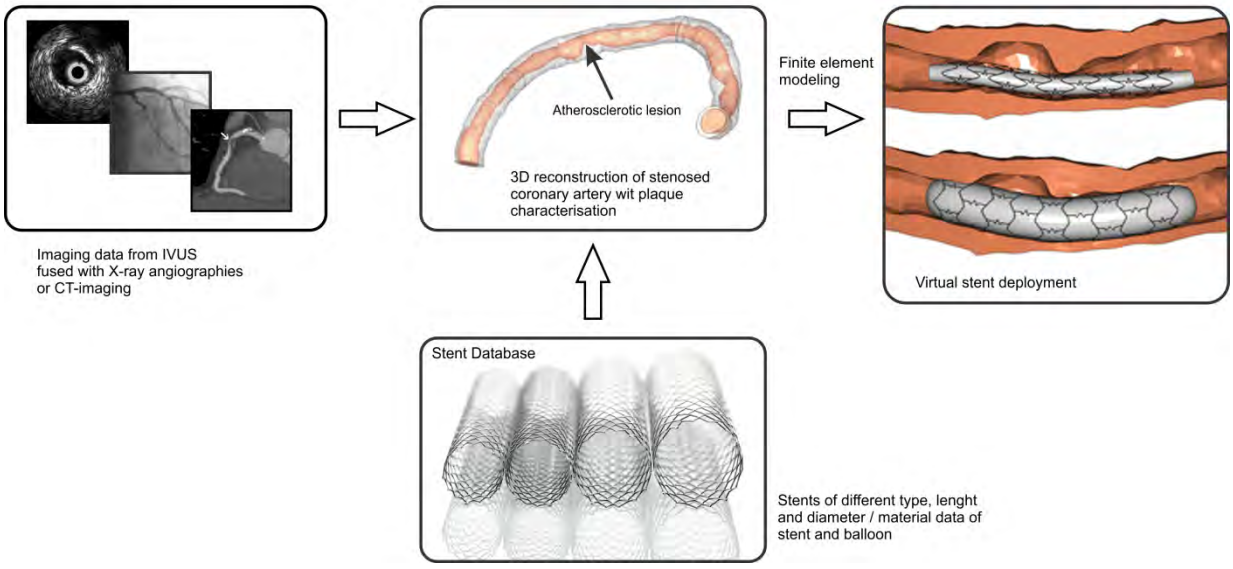

Figure 4. Procedure for virtual stent deployment

In preparation of the numerical model of the stenosed artery, the plaque region is selected. All elements of the arterial wall which form the stenosis are defined as a new region for which separate material properties can be applied. Basis for the element selection is the plaque identification of the segmentation process. In the Figure 4, a half of the stenosed artery model is shown with the defined plaque region.

The placement and adjustment of stent and balloon to artery curvature is realised using the midline of artery in the region of interest. The construction of the artery midline as an auxiliary geometrical measure takes into consideration that the stent can be fitted into the stenosed region. For that purpose, at three or four characteristic cross sections along the artery length in the selected region of interest, the midpoints are constructed which are used for the construction of the midline using a spline function. The bending of the stent according to the midline is done geometrically. The balloon is built as a covering surface around the midline with a diameter 20% smaller than the stent diameter. Figure 5 shows the region of interest with midline and fitting of stent and balloon.

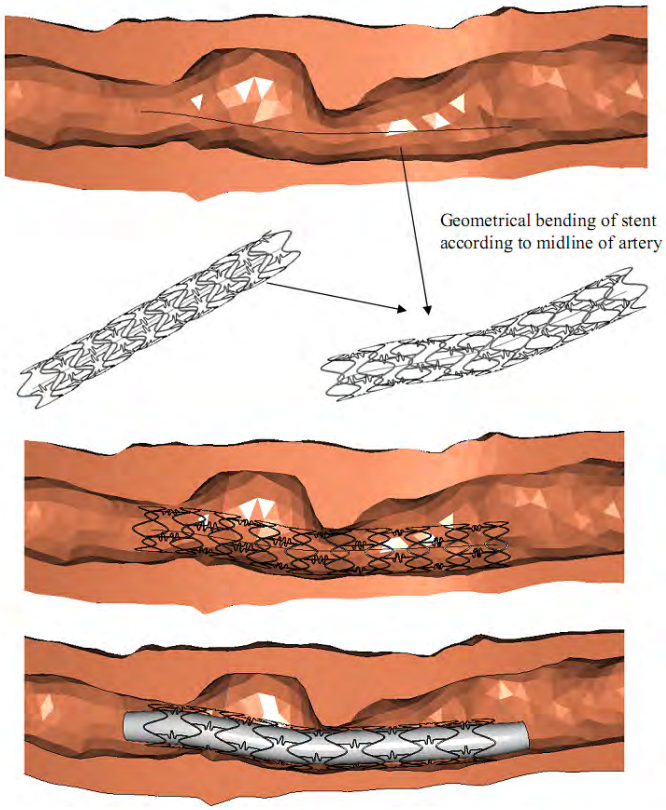

Figure 5. Bending of stent and balloon according to artery curvature

For post-processing of the virtual stenting intervention, the clinician is not only provided with comprehensible animations and graphical outputs showing the process and final state of the implanted device, but with a number of indicators which allow a judgment on the performance of the selected stent and of its interactions with the specific artery. Such indicators include the inflation pressure - lumen area relationship, the final dilation of the artery, stress and strain distributions not only for the stent but also for artery, and the contact stress between stent struts and vessel wall.

4. DISCUSSION AND CONCLUSIONS

We analyse experimental stent testing according to standard ISO 25539-1, Cardiovascular implants - Endovascular devices and computer modeling with plaque formation and progression for specific patient in the coronary arteries. A coupled 3D artery reconstruction from IVUS and Angiography image modalities, with ability of detection of luminal narrowing, on one side, and generating finite element models and processing them, on the other side is described. A few different patients with significant in stent restenosis were analysed. The geometry of the patients for baseline and follow-up has been used with image techniques. We coupled the flow equations with the transport equation applying realistic boundary conditions for each patient.

Blood flow simulation is described with Navier-Stokes and continuity equation. The governing finite element equations used in modeling wall tissue deformation with emphasis on implementation of nonlinear constitutive models are described. The coupling of fluid dynamics and solute dynamics at the endothelium was achieved by the Kedem-Katchalsky equations. The examples with rigid and deformable arterial wall with stented and unstented arteries are presented.

Presented methodologies represent the patient-specific modeling tools which can be used for clinical treatment decisions. Obtained results are very valuable because they make possible to visualize and present spatial distribution of biomechanical quantities which is practically impossible to obtain without modeling.

Stress distribution of the artery wall and stent during expansion of occluded zones is analyzed. Also shear stress distribution before and after stent deployment is compared. From the comparison with the preoperative situation, it is possible to observe how the stent pushes the arterial wall towards the outside allowing the expansion of the occluded artery. Better understand of stent deployment procedure and arterial wall response as well as optimal

stent design can be obtained using computer simulation.

5. ACKNOWLEDGEMENTS

This research is supported from FP7-ICT2007 grant agreement 224297 (ARTreat), HORIZON2020 689068 (SMARTool) and Ministry of Education, Science and Technological Development of Republic Serbia grants: III41007, ON174028.

6. REFERENCES

[1] D. L. Fischman, M. B. Leon, D. S. Baim, R. A. Schatz, M. P. Savage, I. Penn, K. Detre, L. Veltri, D. Ricci, M. Nobuyoshi, M. Cleman, R. Heuser, D. Almond, P. S. Teirstein, R. D. Fish, A. Colo, *A randomized comparison of coronary-stent placement and balloon angioplasty in the treatment of coronary artery disease*. N.Engl.J. Med. 331: (1994) 496−501.

[2] M. C. Morice, P. W. Serruys, J. E. Sousa, J. Fajadet, B. Hayashi, M. Perin, A. Colombo, G. Schuler, P. Barragan, G. Guagliumi, F. Molnàr, *A Randomized Comparison of a Sirolimus-Eluting Stent With a Standard Stent For Coronary Revascularization*, N.Engl. Med 349: (2002) 1315−1323.

[3] V. S. Newman, J. L. Berry, W. D. Routh, C. M. Ferrario, R. H. Dean, *Effects of vascular stent surface area and hemodynamics on intimal thickening*. J. vasc. Interv. Radiol. 7: (1996) 387−393.

[4] T. Murata, T. Hiro, T. Fujii, K. Yasumoto, A. Murashige, M. Kohno, J. Yamada, T. Miura, M. Matsuzaki, *Impact of the cross-sectional geometry of the post-deployment coronary stent on in-stent neoinimal hyperplasia: an intravascular ultrasound study*. Circ. J. 66: (2002) 489−493.

[5] J. Murphy, F. Boyle, *Assessment of the effects of increasing levels of physiological realism in the computational fluid dynamics analyses of implanted coronary stents*. 3th Annual International IEEE EMBS Conference. 2008.

[6] N. DePaola, M. A. J. Gimbrone, P. F. Davies, C. F. Dewey, *Vascular endothelium responds to fluid shear stress gradients*. Arterioscler. Thromb. 12: (1992) 1254−1257.

[7] R. Balossino, F. Gervaso, F. Migliavacca, G. Dubini, *Effects of different stent designs on local hemodynamics in stented arteries*. Journ. of Biomechanics 41: (2008) 1053−1061.

[8] N. Bernard, D. Coisine, E. Donal, R. Perrault, *Experimental study of laminar blood flow through an artery treated by a stent implantation: characterisation of intra-stent wall shear stress*. Journ. of Biomechanics. 36: (2003) 991−998.

[9] M. Gay, L. T. Zhang, *Numerical studies on fluid-structure interactions of stent deployment and stented arteries*. Engineering with Computers. 36: (2009) 61−72.

[10] Y. He, N. Duraiswamy, A. O. Frank, J. E. Moore Jr., *Blood Flow in Stented Arteries:A Parametric Comparison in Three-Dimensions*. Journal of Biomechanical Engineering. 22: (2005) 637−647.

[11] S. Natarajan, Mokhtarzadeh-Dehghan MR, *A numerical and experimental study of periodic flow in a model of a corrugated vessel with application to stented arteries*. Medical Engineering & Physics. 22: (2000) 555–566.

[12] J. F. LaDisa, I. Guler, L. E. Olson, D. A. Hettrick, J. R. Kersten, D. C. Warltier, P. S. Pagel, *Three-Dimensional Computational Fluid Dynamics Modeling of Alterations in Coronary Wall Shear Stress Produced by Stent Implantation.* Annals of Biomedical Engineer. 31 (2003) 972−980.

[13] T. Seo, L. G. Schachter, A. I. Barakat, *Computational Study of Fluid Mechanical Disturbance Induced by Endovascular Stents*. Annals of Biomedical Engineering. 33(4) (2005) 444–456.

[14] A. Tortoriello, G. Pedrizzetti, *Flow-tissue interaction with compliance mismatch in a model stented artery*. Journal of Biomechanics. 37 (2004) 1–11.

[15] J. L. Berry, A. Santamarina, J. E. Moore, S. Roychowdhury, W. D. Routh, *Experimental and Computational Flow Evaluation of Coronary Stents*. Annals of Biomedical Engineering 28: (2000) 386–398.

[16] J. F. LaDisa, L. E. Olson, H. E. Douglas, D. C. Warltier, J. R. Kersten, P. S. Pagel, *Alterations in regional vascular geometry produced by theoretical stent implantation influence distributions of wall shear stress: analysis of curved artery using 3D computational fluid dynamics models.* Biomed Eng Online, 16:5, (2006) 40.

[17] J. F. LaDisa, L. E. Olson, I. Guler, D. A. Hettrick, J. R. Kersten, D. C. Warltier, P. S. Pagel, *Circumferential vascular deformation after stent implantation alters wall shear stress evaluated with time-dependent 3D computational fluid dynamics models*. J. Appl Physiol. 98: (2005) 947−957.

[18] D. Rajamohan, R. K. Banerjee, L. H. Back, A. A. Ibrahim, M. A. Jog, *Developing Pulsatile Flow in a Deployed Coronary Stent*. Journal of Biomechanical Engineering 128: (2006) 347−359.

[19] M. Kojic, N. Filipovic, B. Stojanovic, N. Kojic, *Computer Modeling in Bioengineering:*

Theoretical Background, Examples and Software. John Wiley and Sons, Chichester, England, 2008.

[20] N. Filipovic, S. Mijailovic, A. Tsuda, M. Kojic, *An Implicit Algorithm Within The Arbitrary Lagrangian-Eulerian Formulation for Solving Incompressible Fluid Flow With Large Boundary Motions*. Comp. Meth. Appl. Mech. Engrg. 195: (2006) 6347−6361.

[21] C. A. Taylor, T. J. R. Hughes, C. K. Zarins, *Finite element modeling of blood flow in arteries*, Comp. Meth. Appl. Mech. Engrg. 158: (1998) 155−196.

[22] S. Nanfeng, W. Nigel, H. Alun, T. X. Simon, X. Yun, *Fluid-Wall Modelling of Mass Transfer in an Axisymmetric Stenosis: Effects of Shear-Dependent Transport Properties* 34: (2006) 1119−1128.

[23] N. Filipovic, M. Rosic, I. Tanaskovic, Z. Milosevic, D. Nikolic, N. Zdravkovic, A. Peulic, D. Fotiadis, *ARTreat project: Three-dimensional Numerical Simulation of Plaque Formation and Development in the Arteries*, IEEE Trans Inf Technol Biomed. PMID: 21937352, 2011.

[24] N. Filipovic, *PAK-Athero, Finite Element Program for plaque formation and development.* University of Kragujevac, Serbia, 2013.

ЕКСПЕРИМЕНТАЛНО ТЕСТИРАЊЕ И НУМЕРИЧКО МОДЕЛИРАЊЕ СТЕНТОВА У КОРОНАРНИМ АРТЕРИЈАМА

Сажетак: У раду је приказано експериментално тестирање и нумеричко моделирање стентова са формирањем плака и прогресије за појединачног пацијента на коронарним артеријама. У секцији методе прво је описана процедура експерименталног тестирања стентова. Затим су описане нумеричке методе симулација методом коначних елемената. Струјање крви описано је Навије−Стоксовом једначином и једначином континуитета. Зидови крвних судова су моделирани са нелинеарним високоеластичним материјалним моделом. Спрезање динамике флуида и транспортних једначина на зиду ендотелијуму описано је Кедем−Качалски једначинама. Инфламаторни процес је моделиран додатним реакционо-дифузним једначинама. У секцији резултати приказани су неки примери крутих и деформабилних артеријских зидова са и без стента. Презентован је ефективни напон у самом стенту приликом његове уградње у коронарну артерију. Ови експериментални и нумерички резултати могу допринети бољем разумевању процеса уградње стента и одговора зидова артерија у свакодневној клиничкој пракси.

Кључне речи: тестирање стентова, експериментално, нумерички, симулација уградње стентова, метод коначних елемената.